Interfacial characterization of poly (vinyl alcohol) fibers embedded in a calcium phosphate cement matrix

An experimental and numerical investigation

Paknahad, Ali; Petre, Daniela G.; Leeuwenburgh, Sander C.G.; Sluys, Lambertus J.

DOI
10.1016/j.actbio.2019.06.044

Publication date
2019

Document Version
Accepted author manuscript

Published in
Acta Biomaterialia

Citation (APA)
Paknahad, A., Petre, D. G., Leeuwenburgh, S. C. G., & Sluys, L. J. (2019). Interfacial characterization of poly (vinyl alcohol) fibers embedded in a calcium phosphate cement matrix: An experimental and numerical investigation. *Acta Biomaterialia*, *96*, 582-593. https://doi.org/10.1016/j.actbio.2019.06.044

Interfacial characterization of poly (vinyl alcohol) fibers embedded in a calcium phosphate cement matrix: An experimental and numerical investigation

Ali Paknahad[a,b,*], Daniela G. Petre[a], Sander C.G. Leeuwenburgh[a], Lambertus J. Sluys[b]

[a] *Department of Regenerative Biomaterials, Radboud University Medical Center, Nijmegen, the Netherlands*
[b] *Faculty of Civil Engineering and Geosciences Delft University of Technology, Delft, the Netherlands*

Abstract

Because of their chemical similarity to the mineral phase of bone and teeth, calcium phosphate cements are extensively investigated for applications in biomedicine. Nevertheless, their applicability in load-bearing anatomical sites is restricted by their brittleness. Reinforcement of calcium phosphate cements with polymeric fibers can overcome this mechanical limitation provided that the affinity between these fibers and the surrounding matrix is optimal. To date, the effects of the fiber-matrix affinity on the mechanical properties of fiber-reinforced calcium phosphate cements are still poorly understood. The goal of this study is therefore to investigate the interfacial properties and bond-slip response between the CPC matrix and polymeric fibers. To this end, we selected polyvinyl alcohol fibers as reinforcing agents because of their high strength and stiffness and their effective reinforcement of cementitious matrices. Micromechanical pull-out experiments were combined with numerical simulations based on an dedicated constitutive interfacial law to characterize the interfacial properties of poly (vinyl alcohol) fibers embedded in a calcium phosphate cement matrix at the single fiber pull-out level. The computational model developed herein is able to predict all three main phases of pull-out response, *i.e.* the elastic, debonding and frictional pull-out phases. The resulting interfacial constitutive law is validated experimentally and predicts the pull-out response of fibers with different diameters and embedded lengths.

Keywords: calcium phosphate cements, PVA fiber, pull-out test, fiber-matrix bond strength

*Corresponding author
Email address: a.paknahad@tudelft.nl; ali.paknahad@radboudumc.nl (Ali Paknahad)

1. Introduction

Calcium phosphate cements (CPCs) are widely used in orthopedic and dental surgery due to their chemical similarity to the mineral phase of bones and teeth [1, 2]. Consequently, clinically used CPCs reveal excellent compatibility to bone tissue [3–5]. These biomaterials can be prepared in the operating room and they can be directly injected or molded during surgery into bone defects or gaps between bones and implants [6]. These CPCs are attractive alternatives to the majority of currently available sintered bone substitutes due to their moldability and in-situ hardening properties [7, 8].

CPCs are produced by mixing a precursor powder and liquid phase at different liquid-to-powder ratios (L/P ratio). During this process, calcium phosphate crystals are formed by precipitation which eventually interlock to give mechanical stability to the cement [9]. Despite their widespread usage in orthopedic and dental surgery, currently available CPCs are far from ideal, mainly in view of their poor mechanical properties. Bending strength values of CPCs are indeed reported in the 5–15 MPa range, far below the values reported for cortical bone (about 200 MPa [10]). Morgan et al. [11] investigated damage and fracture properties of carbonated apatite CPCs and reported fracture toughness values of 0.14 MPa $m^{1/2}$ which is considerably lower than the fracture toughness of human cortical bone (2–5 MPa $m^{1/2}$ as reported by Nalla et al. [12]). These limited values of bending strength and fracture toughness of currently available CPCs stress the strong need for the development of CPCs with improved mechanical propertie in terms of enhanced toughness and strength [13]. This toughness of cementitious matrices can be improved most efficiently using reinforcing fibers, as shown for instance by the effective reinforcement of concrete using polymeric fibers. In addition to design criteria such as the amount, dimensions, and mechanical properties of these polymeric fibers, fibers should also be biocompatible for biomedical applications. Generally, polymeric fibers used for biomedical applications are either resorbable or non-resorbable. Resorbable fibers made of natural or synthetic polymers such as collagen, polylactic acid (PLA), poly(lactic-co-glycolic acid) (PLGA), or polycaprolactone (PCL) are too weak to reinforce CPCs efficiently [14, 15]. On the contrary, non-resorbable fibers composed of polyamides, carbon or glass reinforce cementitious matrices more efficiently due to their higher tensile strength and stiffness [1].

PVA fibers are a particularly promising fiber type for reinforcement of CPCs because of their high modulus of elasticity and tensile strength. Moreover, their strong affinity for hydrophilic cementitious was already exploited effectively for reinforcement of other cementitious matrices such as concrete [16]. Finally, PVA is regarded as a biocompatible polymer in the biomedical field, as

shown by its use in various applications in biomedicine [17]. In view of these beneficial properties, PVA fibers have been recently introduced into CPCs, thereby transforming brittle CPCs to ductile and tough fiber-reinforced calcium phosphate cements (FRCPCs) [18].

In order to describe the mechanical behavior of fiber-reinforced CPCs three main phases can be discerned, *i.e.* the CPC matrix, fibers, and the fiber-matrix interface. While the matrix and fiber phases of fiber-reinforced CPCs are adequately understood, the effect of the interface between polymeric fibers and the matrix of CPCs is still poorly understood [19]. This interface behavior is dictated by chemical, frictional, and mechanical interactions between the matrix and embedded fibers [20, 21]. Stresses are transferred from the matrix to the fibers through this fiber-matrix interface. Consequently, the mechanical properties of fiber-reinforced CPCs can only be optimized when their fiber-matrix interface is fully understood.

Experimental single-fiber pull-out tests are the most common micromechanical tests to assess the fiber-matrix affinity [22, 23]. From these tests, key parameters which characterize the pull-out response can be derived in a quantitative manner including the critical fiber embedded length. This parameter is defined as the longest fiber length that can be pulled out of its surrounding matrix without any rupture [24].

Recently, single-fiber pull-out behavior has also been studied analytically and numerically [25–30]. Single-fiber pull-out tests using PVA fibers embedded in a concrete matrix were performed and analyzed at both quasi-static and high pull-out rates by Scheffler et al. [28]. They investigated both as-received and surface-treated PVA fibers and demonstrated that removal of fiber coatings can affect the interfacial mechanical bonding between the PVA fiber and the concrete matrix. An analytical micromechanical model for polymeric fibers of hydrophobic and hydrophilic nature embedded in a concrete matrix was developed by Lin et al. [29]. This model included the effect of chemical bonding and slip-dependent interfacial properties to provide a more realistic representation of the fiber-matrix interfacial interactions. Breitenbucher et al. [30] analyzed the pull-out response of steel fibers considering different inclinations and concrete matrix strength. They developed an analytical model for hooked-end fibers considering the anchorage effect and proposed an interface law for pull-out behavior of straight fibers.

Although numerous studies have been dedicated to fiber reinforcement of cementitious matrices used in civil engineering [30–36], the interface behavior of polymeric fibers and biomedical cements is still hardly investigated. Herein, we study the pull-out response of PVA fibers from a CPC matrix

both experimentally and numerically for different fiber embedded lengths and diameters. We use two types of interfacial constitutive laws to represent the fiber-matrix interface properties in our numerical model. The first suggested interfacial constitutive law can predict only the elastic and frictional pull-out stages. Here we ignore the debonding stage. This could be a valid approximation specifically for fibers with relatively small diameters and embedded lengths. In previous literature, usually the debonding stage is either ignored or assumed with constant frictional shear stress. In the experimental data presented in this paper we noticed a distinct debonding stage that is also slip-dependent. Therefore, we suggest an advance interfacial constitutive law that is able to capture the complete pull-out process including a slip-dependent debonding stage.

Specifically, we i) present a novel experimental protocol to assess the affinity between PVA fibers and the surrounding CPC matrix by means of single-fiber pull-out tests; (ii) we determine the critical embedded length for PVA fibers with two different diameters and correlate the work of pull-out with the embedded length; and (iii) we design a numerical model with a predictive interfacial constitutive law which describes the three main phases of single-fiber pull-out, *i.e.*, the elastic, debonding and frictional stages. This numerical model is validated with our experimental data.

2. Experimental studies

2.1. Single-fiber pull-out test

During a pull-out test, a single fiber is pulled out from the surrounding cement matrix and the pull-out force versus the displacement is measured. Generally, the pull-out response strongly depends on the matrix composition, chemical properties of the fiber, and fiber geometry including fiber diameter and fiber embedded length. A possible simplification is to assume that the fiber is pulled out from the matrix with a constant frictional force along the entire fiber-matrix interface [25]. In this case the frictional shear stress τ is set equal to a constant value (τ_0) and it is independent of fiber slippage. This assumption may be valid for specific types of matrix and fibers [37, 38]. However, the interfacial shear strength τ is more often a function of fiber slippage [28, 39]. Figure 1 shows a schematic drawing of pull-out responses with constant and slip-dependent frictional force on the interface. Here, $P_{\max}, P_{\max l}, P_{\mathrm{db}},$ and l_{e} represent the maximum pull-out load, local maximum pull-out force, debonding pull-out force, and the embedded length, respectively. Fiber pull-out can

lead to a slip-softening, constant friction, or slip-hardening behavior depending on the fiber-matrix interface adhesion, fiber surface roughness, and the relative properties of matrix and fiber [39].

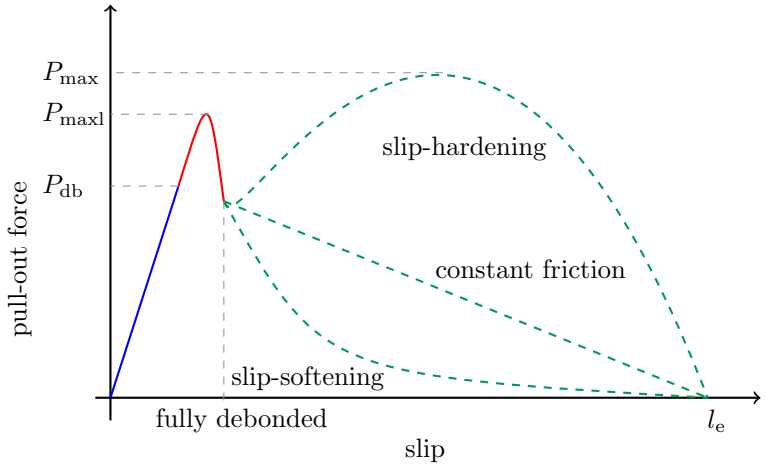

Figure 1: Schematic representation of pull-out response with slip-softening, constant friction, and slip-hardening behavior

2.2. Experimental single-fiber pull-out tests

To investigate the affinity between PVA fibers and the CPC matrix, two types of PVA fibers with diameters of 200 and 100 μm were pulled out from CPC at embedded lengths between 2 and 10 mm. Fiber diameter and embedded length are two main parameters that can affect the bond strength between fiber and matrix. The types and properties of the PVA fibers used herein (Kuraray Co., Ltd.) are listed in Table 1.

Table 1: Properties of the PVA fibers employed in the experimental tests

Diameter (μm)	Length (mm)	Tensile strength (GPa)	Modulus (GPa)	Poisson ratio
200	18	1.0	27	0.2
100	12	1.2	28	0.2

The physical properties and specimen geometry of the CPC used as matrix for all experiments are listed in Table 2. The powder phase of the CPC consists of 100% α-tricalcium phosphate

(α-TCP) (CAM Bioceramics, Leiden, the Netherlands), while the liquid phase consists of a 4 wt% $NaH_2PO_4.2H_2O$ (Merck, Darmstadt, Germany) aqueous solution.

Table 2: Properties of CPC specimens

Matrix	Specimen diameter (mm)	Specimen height (mm)	Flexural modulus (GPa)	Flexural strength (MPa)	Poisson ratio
CPC	6	$2-10 \pm 0.5$	2.5 ± 0.6	6.6 ± 1.6	0.2

Specimens were prepared by adding the liquid phase to the CPC powder at a liquid-to-powder ratio of 1:2. CPC powder and liquid phase were thoroughly mixed together for 1 minute until a paste was formed. Afterwards, the paste was placed in molds with an inner diameter of 6 mm 3-D printed from dissolvable PVA (Ultimaker 2+). Cylindrical molds were prepared at different heights to allow fiber placement at different embedded lengths ($2, 4, 6, 8$ and 10 mm) using guide notches. Subsequently, the specimens were clamped and allowed to set for 24 hours at room temperature. Figure 2 shows a schematic drawing of the mold (left) and a 3-D printed mold (right) with width and length of 10 mm and height of 4 mm.

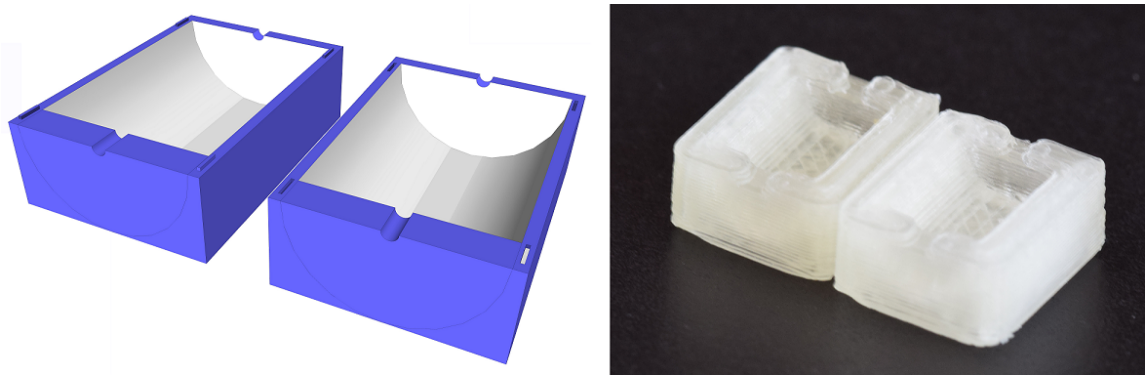

Figure 2: Schematic drwaing of the mold (left) and a 3-D printed mold (right)

After an initial setting time of 24 hours, the specimens were immersed in distilled water for 24 hours to dissolve the PVA. Subsequently, the specimens were immersed in a phosphate-buffered saline solution (PBS) and placed on a shaker table set at 120 rpm in an incubator at 37° C for 72 hours to allow the CPC to fully cure. Figure 3 shows a typical specimen.

Figure 3: An experimental specimen with embedded PVA fiber

Before the pull-out tests, all specimens were glued (Pleximon) to a solid base (3-D printed from PLA) and dried at room temperature. Finally, the dried specimens were again immersed in the PBS solution and placed on a shaker table set to 120 rpm in an incubator at 37° C for 30 min to allow for complete hydration. Pull-out tests were performed immediately after removing the specimens from the PBS solution to mimic physiological conditions. A representative sketch of the pull-out test setup is illustrated in Figure 4.

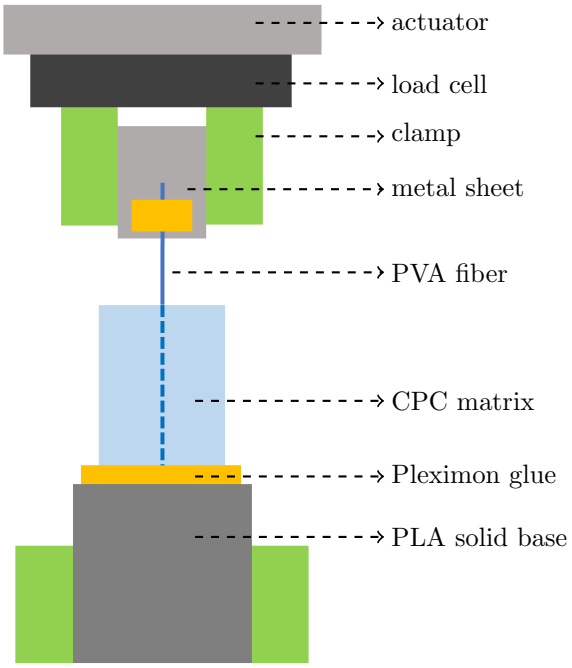

Figure 4: A schematic sketch of the pull-out test setup

Using a tensile bench (LLOYD material testing, LS1 series), the pull-out load was applied in the fiber axial direction at a crosshead speed of 1 mm/min. A data collection frequency of 16 kHz was used to record the experimental data points. Fiber surface abrasion before and after the pull-out test was analyzed using the scanning electron micrographs (SEM). Samples were coated with a 10 nm chromium layer and images were obtained at 5 kV. To check the fiber location and incidence of damage during the pull-out test, samples were scanned using nano-CT (Phoenix NanoTom M, General Electric, Wunstorf, Germany). Images were acquired using a voxel size of 3.36 μm, X-ray source of 60 kV/ 140 μA, and exposure time of 500 ms without the application of a filter.

2.3. Results and discussion

2.3.1. Pull-out behavior of 200 μm thick PVA fibers

PVA fibers with a diameter of 200 μm were pulled out from CPC matrix at embedded lengths of $2, 4, 6, 8$, and 10 mm (see Figure 5). All experimental data were examined for outliers using Tukey's criteria based on the maximum pull-out force. The initial parts of the curves (before the first local maximum) for $2, 4, 6,$ and 8 mm embedded length are very similar. Their initial slopes are

very close, which means that the effective stiffness of the specimens does not show any significant dependence on the embedded length, while the peak load increases with increasing embedded length. The pull-out force slip curves show nonlinear behavior after the initial elastic phase and also multiple maximum peaks in the post-debonding region. This evidences that the interfacial frictional stress in these tests is not constant but varies with embedded length [40].

For embedded lengths of $4, 6$, and 8 mm the maximum peak load occurred somewhere in the post-debonding region, while for cases with 2 mm embedded length the maximum peak load occurred at the end of the elastic or frictional-free phase. This proves that the amount of mechanical interlocking and chemical adhesion between the PVA fiber and the CPC matrix during pull-out of fibers with 2 mm embedded length is much lower compared to the pull-out of fibers with $4, 6$, and 8 mm embedded lengths. This is expected due to the small interfacial surface area between fiber and matrix. In other words, the area under a pull-out force displacement curve of fibers with 2 mm embedded length, usually called "pull-out work" [41], reduces significantly compared to the pull-out of fibers with $4, 6$, and 8 mm embedded lengths. Pull-out work generally increases with increasing embedded lengths (see Figure 5f). To determine the minimum efficient fiber embedded length for this thickness, where the pull-out response is close to a friction-less situation, fiber pull-out tests with embedded length shorter than 2 mm would be necessary. During the friction-less response the pull-out process ends after the debonding stage. However, these tests were not feasible for the current experimental setup due to technical limitations.

For fibers with 10 mm embedded length, the pull-out process was not completed and most fibers broke after reaching the ultimate load. According to the results shown in Figure 5, the critical embedded length (l_c) of PVA fibers with $200\,\mu$m diameter is approximately between 8 to 10 mm. The critical embedded length, defined as the maximum fiber embedded length for a fiber to be pulled out from a matrix without rupture, is a prominent interface parameter that can strongly affect the pull-out response and hence the efficiency of the interfacial properties in FRCPC.

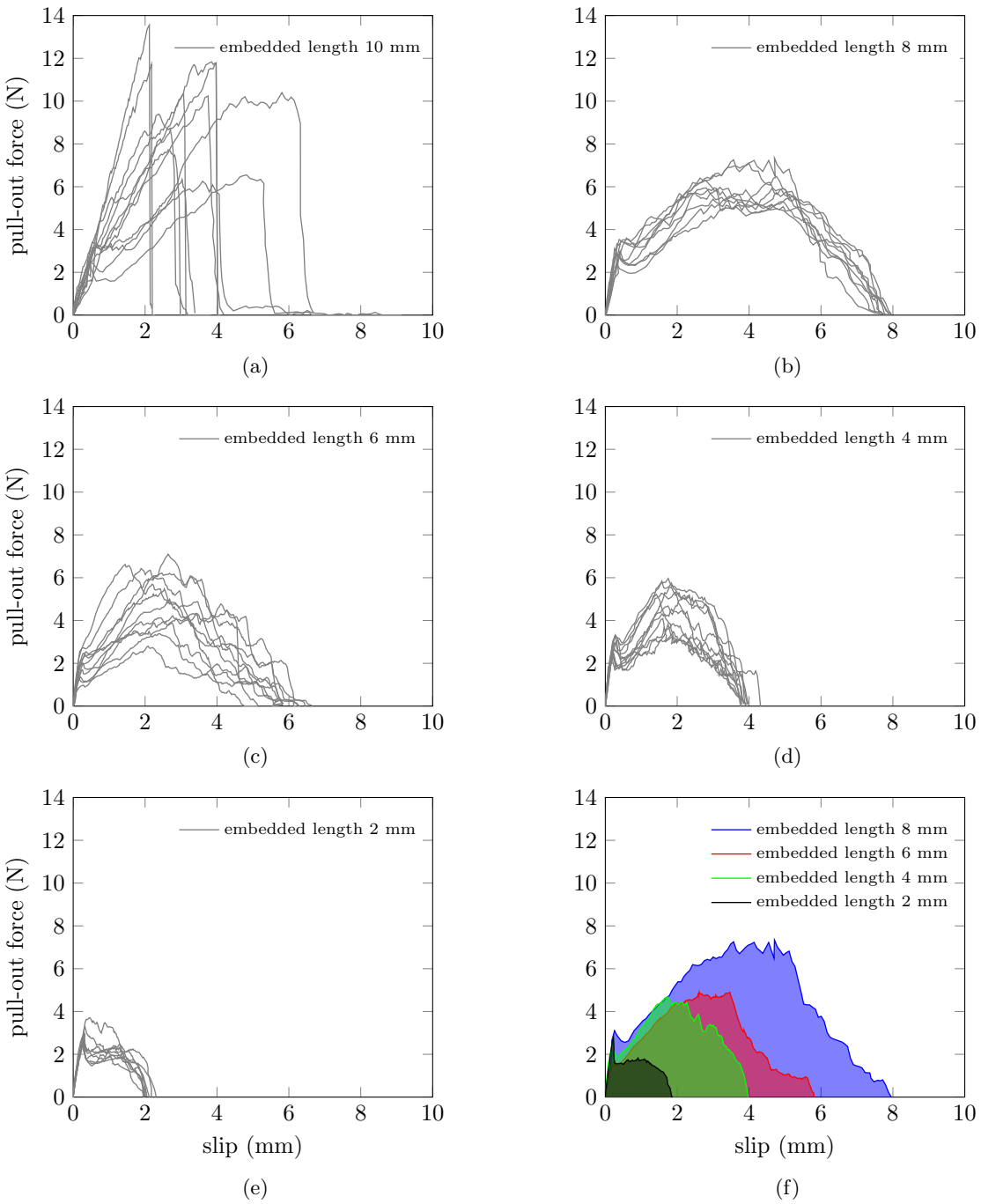

Figure 5: Force-displacement curves for pull-out of 200 μm thick PVA fibers from CPC matrix at embedded lengths of a) $l_e = 10$ mm, b) $l_e = 8$ mm, c) $l_e = 6$ mm, d) $l_e = 4$ mm, e) $l_e = 2$ mm and f) effect of fiber embedded length on pull-out work

As depicted in Figure 6, a typical pull-out force-displacement curve includes three main phases. The first phase represents the initial elastic stretching of the part of fiber that is not embedded (the fiber-free length). Subsequently, the debonding phase starts and continues until reaching a local peak load accompanied by clear load drop to the point of full debonding. Due to deformability of the PVA fibers [28, 42], the starting point of debonding phase and local maximum load are difficult to distinguish. These two points are very close and usually the starting point of the debonding phase is considered to be directly after the first local maximum load [28]. The load drop after the first peak load corresponds to chemical debonding since this phase would not occur if only frictional bonds are formed between the fiber and the matrix. In fact, the load drop corresponds to the transition from the debonding phase (with both chemical and frictional bonds) to the final, third phase with frictional bonds only [29].

Non-linear behavior was observed in the frictional pull-out phase. This so-called slip-hardening behavior can be observed especially for PVA fibers and is attributed to fiber surface abrasion during the fiber pull-out process. Frictional bonds can significantly increase due to the fibrillation of fiber surface; this is considered to be one of the main mechanisms of slip-hardening [39, 40].

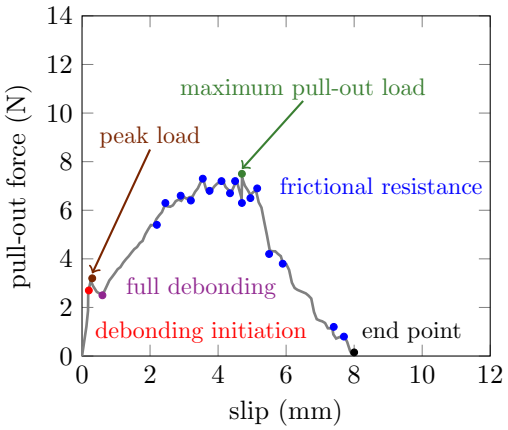

Figure 6: Typical pull-out force vs. slip curve obtained during pull-out of a PVA fiber embedded in CPC matrix ($d_f = 200\,\mu$m, $l_e = 8$ mm)

Figure 7 shows SEM of the PVA fibers with $200\,\mu$m diameter before and after the pull-out test. In Figure 7 fiber surface abrasion upon pull-out is evident. This observation explains the various local maxima and frictional pull-out resistance in the pull-out force-slip curves (see blue

points, Figure 6).

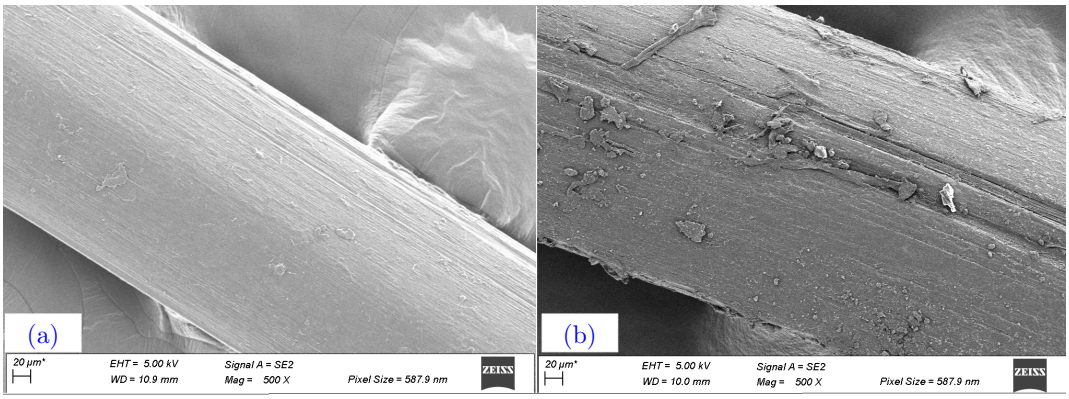

Figure 7: SEM images of PVA fibers, $d_f = 200\,\mu$m a) before and b) after the pull-out test

Nano-CT imaging of the fiber-matrix interface after fiber pull-out indicates that no matrix defects are observed (see Figure 8). Both matrix and fiber remained intact until the end of the test and interface breakage (*i.e.* tunneling) is the only dominant phenomenon during the pull-out process. In addition, Figure 8 shows an intact and dense cement paste surface around the fiber, without voids or noticeable cracks.

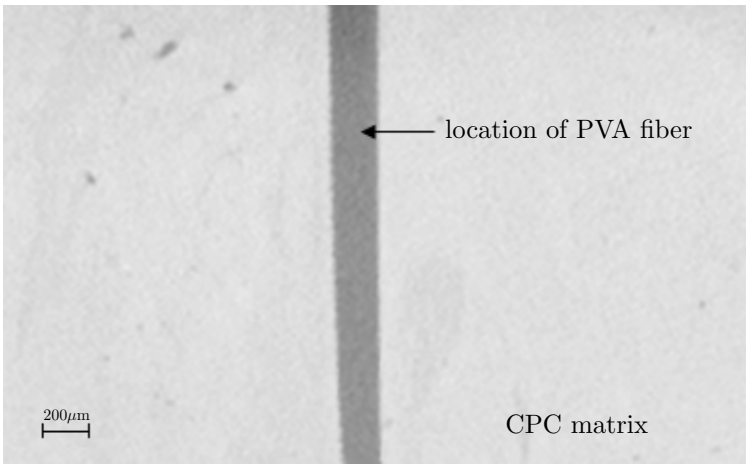

Figure 8: Nano-CT of the fiber-matrix interface after fiber pull-out ($d_f = 200\,\mu$m, $l_e = 6$ mm)

2.3.2. Pull-out behavior of $100\,\mu m$ *thick PVA fibers*

PVA fibers with a diameter of $100\,\mu$m were pulled out from the CPC matrix at embedded lengths of $2, 4$, and 6 mm (see Figure 9). For fibers embedded for 6 mm in CPC, similar to PVA fibers with $200\,\mu$m diameter and 10 mm embedded length, almost all fibers broke immediately after the maximum peak load was reached. This evidences that the strength of mechanical interlock between these PVA fiber and CPC matrix is stronger than the fiber tensile strength.

Based on these results the critical embedded length (l_c) for a PVA fiber with $100\,\mu$m diameter is estimated approximately between 6 and 4 mm. Figure 9d compares the total pull-out work for fibers of 100 and $200\,\mu$m .The pull-out work increases with increasing diameter, since the frictional and chemical interfacial bonding between the fiber and the matrix increase due to the larger fiber circumferential surface.

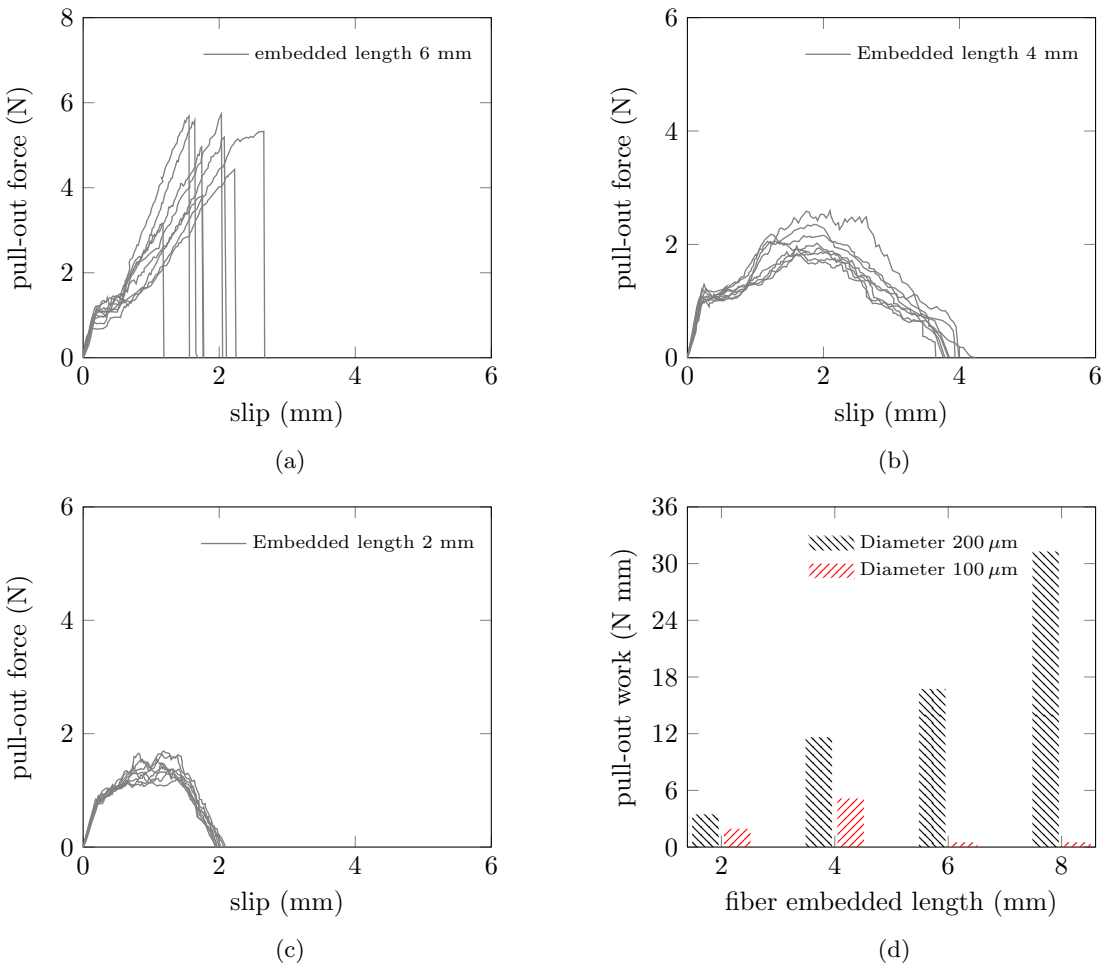

Figure 9: Force-displacement curves for pull-out of 100 μm thick PVA fibers from CPC matrix at embedded lengths of a) $l_e = 6$ mm, b) $l_e = 4$ mm, c) $l_e = 2$ mm and d) effect of fiber diameter on pull-out work

A summary of all experimental results is listed in Table 3. In this table l_e, $F_{\text{max-b}}$, F_{max}, and W represent the fiber pull-out lengths, first local peak load in the debonding phase, the maximum peak load, and pull-out work, respectively.

Table 3: A summary of experimental results

Fiber diameter (μm)	l_e (mm)	$F_{max\text{-}b}$ (N)	F_{max} (N)	W (N mm)	Pull-out status	Number of specimens	Number of fiber ruptures	Maximum load
200	10	8.6 ± 2.4	–	–	Fiber breakage	15	11	–
200	8	2.9 ± 0.4	5.9 ± 0.6	31.3 ± 2.8	Fiber pull-out	15	4	Frictional phase
200	6	2.3 ± 0.6	4.7 ± 1.3	16.8 ± 4.1	Fiber pull-out	16	1	Frictional phase
200	4	2.7 ± 0.3	4.3 ± 0.8	11.6 ± 2.1	Fiber pull-out	18	–	Frictional phase
200	2	2.5 ± 0.4	2.1 ± 0.2	3.5 ± 0.5	Fiber pull-out	15	–	End of elastic phase
100	6	–	–	–	Fiber breakage	14	12	–
100	4	1 ± 0.09	1.9 ± 0.2	5.1 ± 0.6	Fiber pull-out	15	3	Frictional phase
100	2	1 ± 0.05	1.6 ± 0.1	1.9 ± 0.1	Fiber pull-out	16	–	Frictional phase

3. Numerical modeling

In this section, we propose a finite element (FE) numerical model to gain insight into the fiber-matrix interactions during the pull-out process. The goal here is to determine an interfacial constitutive law that represents the fiber-matrix interface properties as observed experimentally.

The CPC matrix and the PVA fiber are discretized by standard continuum elements. To introduce the fiber-matrix interface properties, we employed zero-thickness interface elements with a traction separation law (TSL). A schematic discretization of continuum and zero-thickness interface elements is depicted in Figure 10.

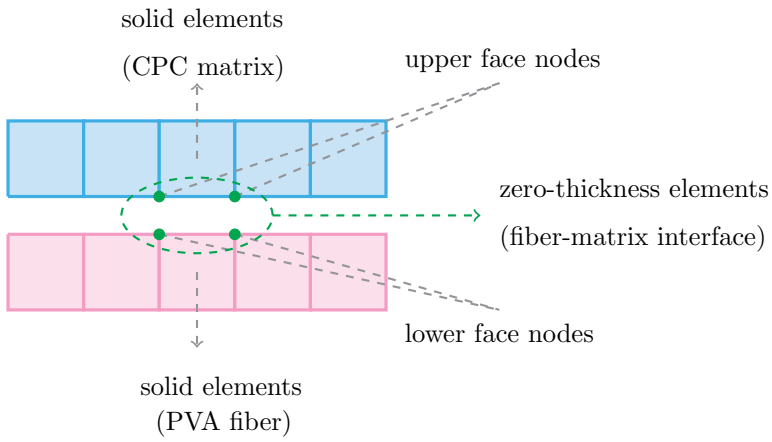

Figure 10: Schematic FE discretization of fiber, matrix and fiber-matrix interface elements

The modeling of the interface was done by means of explicit interface elements because in the single fiber pull-out analysis the location of the interface elements was known. To numerically simulate the fiber pull-out process, the following assumptions were made:

- Crack initiation starts after the local maximum load. Therefore, the first and second kinks in the pull-out force-slip curves (see Figure 6), which represent the starting point of debonding phase and the local maximum load, respectively, were considered equal.

- Based on nano-CT observations, matrix damage, fiber damage, and the effect of fiber surface abrasion were neglected. Therefore, fiber and matrix were considered as linear elastic materials.

The non-linear process is concentrated at the fiber-matrix interface. The constitutive equations can be defined as follows:

$$\boldsymbol{\sigma}_{\mathrm{m}} = \mathbf{D}_{\mathrm{m}}\boldsymbol{\varepsilon}_{\mathrm{m}} \tag{1}$$

$$\dot{\mathbf{t}}_{\mathrm{int}} = \mathbf{T}[\![\dot{\mathbf{u}}_{\mathrm{int}}]\!] \tag{2}$$

$$\boldsymbol{\sigma}_{\mathrm{f}} = \mathbf{D}_{\mathrm{f}}\boldsymbol{\varepsilon}_{\mathrm{f}} \tag{3}$$

where $\mathbf{T}$ denotes the cohesive tangent matrix and $\mathbf{D}_{\mathrm{m}}$ and $\mathbf{D}_{\mathrm{f}}$ are the tangent stiffness matrices for matrix and fiber, respectively. Also $[\![\dot{\mathbf{u}}_{\mathrm{int}}]\!]$ indicates the rate form of displacement jump between the upper and lower faces of the interface element (see Figure 10). The displacement jump in the pull-out study represents the fiber slippage and can be formulated as:

$$[\![\mathbf{u}_{\mathrm{int}}]\!] = \mathbf{N}_{\mathrm{int}}(\mathbf{u}^{+} - \mathbf{u}^{-}) \tag{4}$$

where $\mathbf{u}^{+}$ and $\mathbf{u}^{-}$ represent the nodal displacements on the upper and lower edges of the interface elements and $\mathbf{N}_{\mathrm{int}}$ corresponds to the shape functions of the interface elements.

The experimental results clearly revealed three main stages of the pull-out process. In most of previous studies, the debonding stage was ignored and it was assumed that the frictional pull-out stage starts immediately after the elastic phase. This assumption is valid for PVA fibers with small diameters and high aspect ratios for three reasons [28, 42, 43]. First, relative slippage between the fiber and the matrix in the debonding phase is usually small compared to the elastic and

frictional phase. This is more significant when the embedded length of the fiber is also small. This observation can be evidenced by studying the experimental pull-out results for PVA fibers with 200 and 100 μm diameters (see Figure 5 and 9). Second, it is not straightforward to define the starting and end points of the debonding stage for small polymeric fibers like PVA fibers. For reasons of simplicity, this phase is usually ignored in the literature [28, 42]. Third, it is clear that the quality of the debonding phase directly depends on the fiber surface coating. Usually, industrial fibers are used with an as-received surface coating and less attention is paid to the role of fiber surface treatment in the pull-out process. Therefore, the effect of fiber coating on the debonding stage is rarely considered in numerical studies. The frictional pull-out process can be approximated by slip-hardening behavior following a quadratic function. It is assumed that during the pull-out test the interfacial shear stress between the PVA fiber and the CPC matrix may first increase due to the accumulation of fiber debris.

Two types of TSLs are proposed herein. In the first one we ignore the debonding stage and in the second one we consider all three stages of the pull-out process.

The first TSL describes two phases of the pull-out process. The elastic phase with a linear function and the frictional phase with a quadratic function according to:

$$\tau(s) = \begin{cases} Gs & 0 \leq s \leq s_0 \\ \\ d_{\mathrm{f}} \left(\gamma_2 (s - s_0)^2 + \gamma_1 (s - s_0) \right) + \tau_{\max} & s > s_0 \end{cases} \tag{5}$$

where G is the corresponding relative bond modulus, s is the fiber slippage, s_0, γ_2 and γ_1 represent the starting point of sliding and parameters controlling the ascending branch of the pull-out curve, respectively, and $\tau_{\max}$ is the maximum bond strength of the interface.

Due to symmetry, we constructed a two-dimensional axisymmetric FE model. The only source of nonlinearity comes from the interface behavior. In the simulations, we discretized the region next to the interface with a finer mesh compared to the rest of the domain. The boundary conditions and a typical mesh discretization are shown in Figure 11.

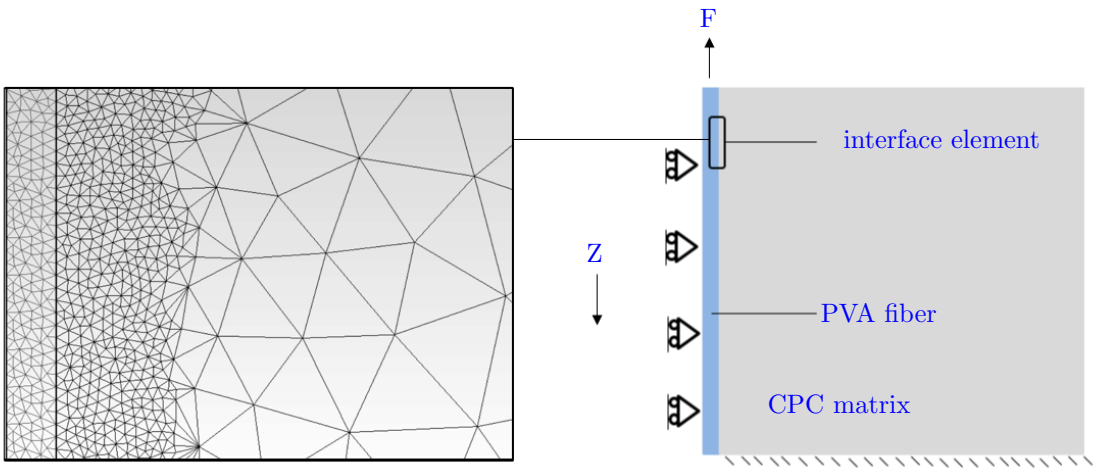

Figure 11: Schematic FE discretization of fiber, matrix and fiber-matrix interface elements

Furthermore, we assumed that the normal stress along the PVA fiber does not exceed its material ultimate strength and therefore the PVA fiber will not break before it pulls out from the CPC matrix. To compare the model prediction with experimental data, a representative average curve for each set of experiments was interpolated using B-splines. We tuned the model parameters such that the best fitted curve with regards to the average experimental result was obtained. We selected the three main points of the pull-out curve, *i.e.* the first peak load, the maximum pull-out load, and the end point of the frictional phase for the model calibration and the best fitting procedure.

The model variables are tuned for the pull-out process of the PVA fiber with 200 μm diameter and 8 mm embedded length and the results is depicted in Figure 12a. The numerical pull-out prediction with these calibrated parameters and the same diameter but now for PVA fibers with 6 and 4 mm embedded lengths are presented in Figure 12b and 12c. The average curves and experimental result are defined with blue lines and gray highlighted bands, respectively.

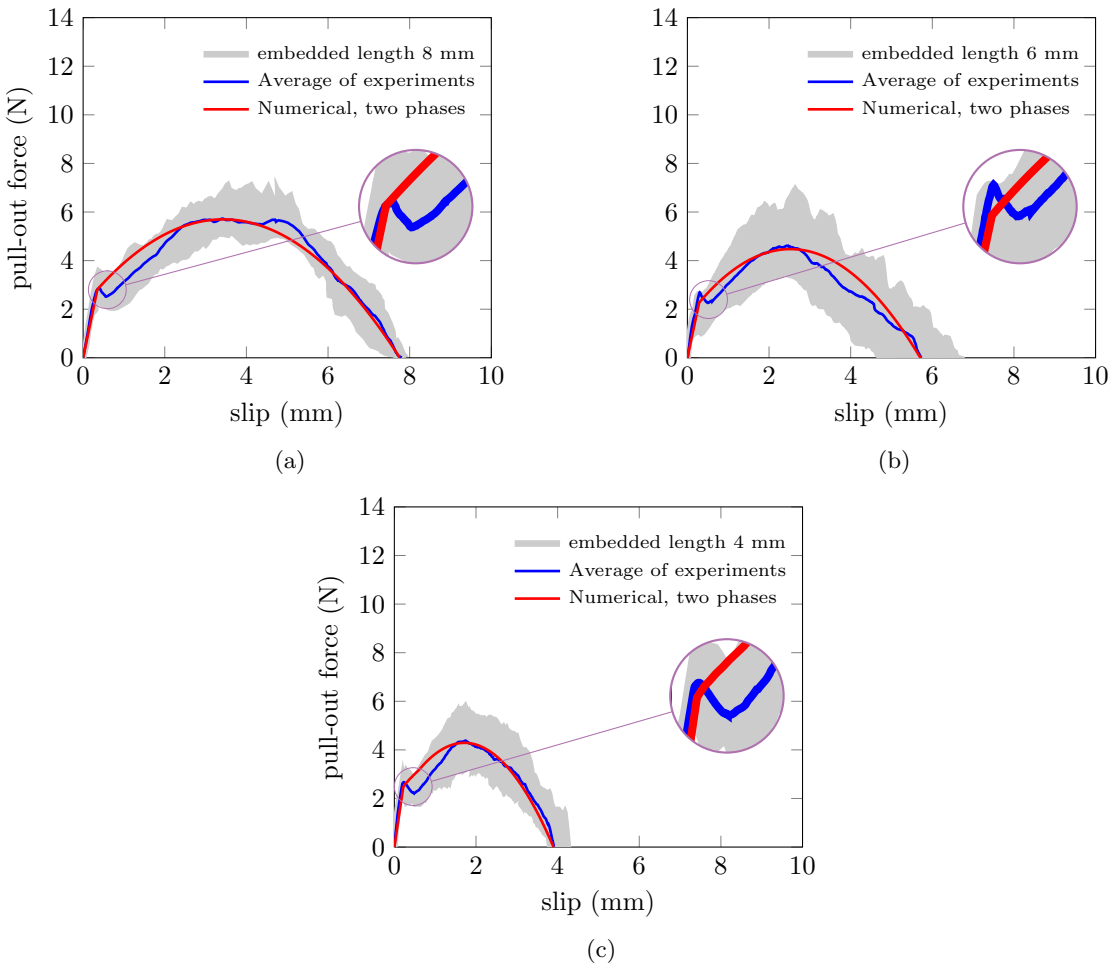

Figure 12: Numerical prediction including two-phase traction separation law for the PVA fiber pull-out test, $d_\mathrm{f} = 200\,\mu$m, a) $l_\mathrm{e} = 8$ mm, b) $l_\mathrm{e} = 6$ mm, c) $l_\mathrm{e} = 4$ mm

Furthermore, for the PVA fiber with $100\,\mu$m diameter, the numerical model parameters were calibrated for the 4 mm embedded length. Figure 13 shows the prediction for the 2 mm embedded length using the same parameters.

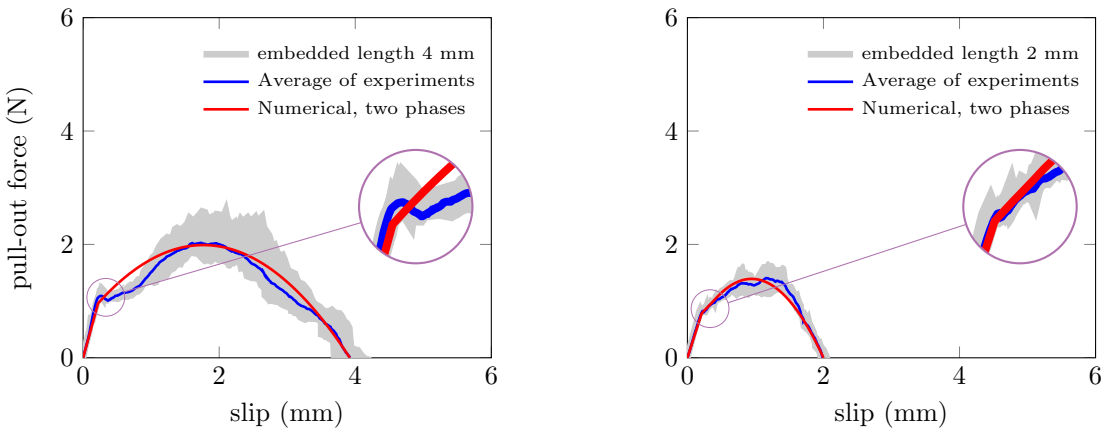

Figure 13: Numerical prediction including two-phase traction separation law for the PVA fiber pull-out test, $d_\mathrm{f} = 100\,\mu$m, $l_\mathrm{e} = 4$ mm (left) and $l_\mathrm{e} = 2$ mm (right).

We observed a strong agreement between the calculated pull-out curves using the numerical model with the proposed two-phase TSL and the experimental data. However, the proposed two-phase TSL in Equation 5 does not capture the debonding stage, but it still can reasonably predict the general trend of the pull-out response.

In our pull-out tests for PVA fibers with 200 and 100 μm diameters, the debonding phase is significant and cannot be excluded from the pull-out analysis as one could do for fibers with small diameters. In fact, all three main stages of the pull-out process can be clearly distinguished from each other. Consequently, the load drop after the first local peak load and during the chemical and frictional debonding stages cannot be ignored. For this reason, a model with a more precise prediction and the ability to mimic the complete pull-out process is required. In this regard, a more advanced version of the TSL that includes all three pull-out phases (namely the elastic, debonding and the frictional pull-out stage) can be formulated as follows:

$$\tau(s) = \begin{cases} Gs & 0 \le s \le s_0 \\ \tau_\mathrm{max}\,\exp\left(\dfrac{s_0 - s}{d_\mathrm{f}\,\gamma_0}\right) & s_0 \le s \le s_1 \\ d_\mathrm{f}\left(\gamma_2 (s - s_1)^2 + \gamma_1 (s - s_1)\right) + \tau_\mathrm{max}\,\exp\left(\dfrac{s_0 - s_1}{d_\mathrm{f}\,\gamma_0}\right) & s > s_1 \end{cases} \tag{6}$$

This version of the TSL employs a linear function for the elastic phase, a descending exponential and slip-dependent function for the debonding stage, and a quadratic function for the frictional pull-out phase.

In Equation 6, G is the corresponding relative bond modulus, and s_0 and s_1 are the starting point of the debonding phase and the sliding phase, respectively. Parameters controlling the descending branch of the pull-out curve in the debonding stage and the ascending branch in the pull-out stage are defined by γ_0, γ_1, and γ_2. Similar to previous simulations, we selected the first peak load, the maximum pull-out load and the end point of the frictional phase as criteria to calibrate the model and find the best fitted numerical curve with regards to the average of the experimental data. The same numerical setup used previously was employed for the three-phase model (see Figure 11). Figure 14 shows the numerical results for the PVA fiber pull-out response with 200 μm diameter and three different embedded lengths. The results of the numerical pull-out analysis for the PVA fiber with 100 μm diameter and two different embedded length are presented in Figure 15. For the PVA fiber with 200 and 100 μm diameters, the model parameters in Equation 6 are tuned for 8 and 4 mm embedded lengths, respectively.

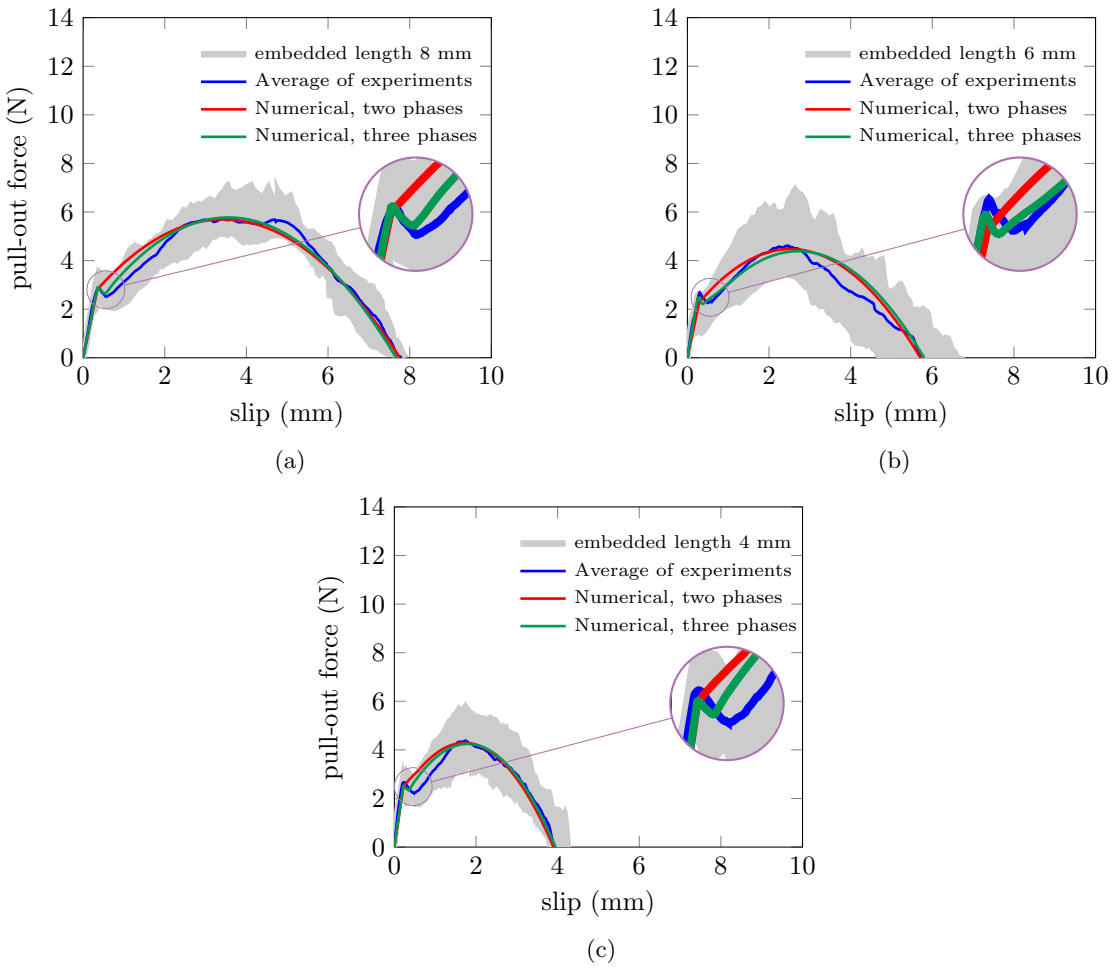

Figure 14: Numerical prediction including three-phase traction separation law for the PVA fiber pull-out test, $d_\mathrm{f} = 200\,\mu$m, a) $l_\mathrm{e} = 8$ mm, b) $l_\mathrm{e} = 6$ mm, c) $l_\mathrm{e} = 4$ mm

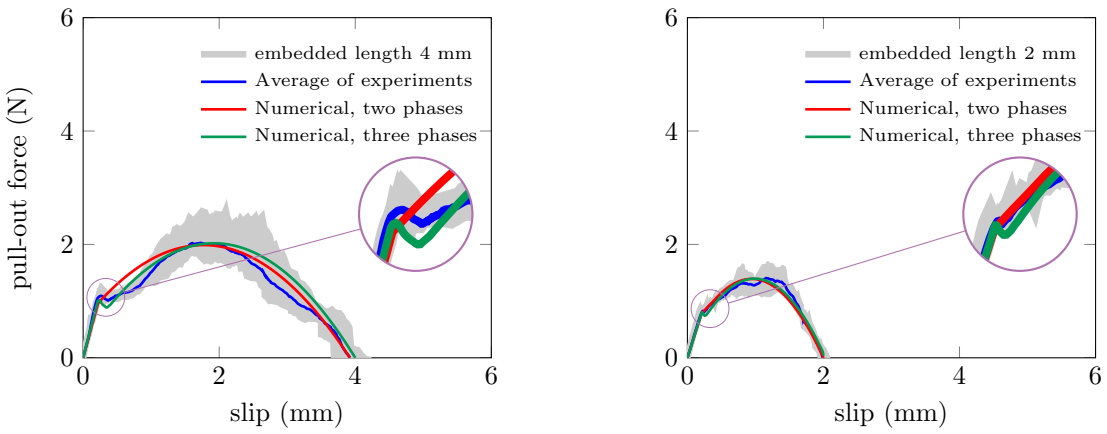

Figure 15: Numerical prediction including three-phase traction separation law for the PVA fiber pull-out test, $d_\mathrm{f} = 100\,\mu$m, $l_\mathrm{e} = 4$ mm (left) and $l_\mathrm{e} = 2$ mm (right).

A better agreement between numerical and experimental data is clearly observed compared to the two-phase model. The three-phase TSL enables the description of the slip-dependent debonding stage and predict the complete pull-out response for different fiber diameters and embedded lengths. It should be highlighted that the effects of chemical and frictional bond strength parameters during the debonding phase were implemented in both models through the model parameters γ_0, γ_1, and γ_2. In addition, the value of fiber diameter d_f is factored out of the TSL model parameters to stress that the fiber diameter strongly affects the interfacial constitutive law.

4. Conclusions

To investigate the fiber-matrix interface properties of PVA fibers embedded in a CPC matrix, we performed experimental single-fiber pull-out tests for fibers with two different diameters (200 and 100 μm) and various embedded lengths between 2 and 10 mm. We determined the critical embedded length for both fiber diameters as the crucial interface parameter governing the pull-out response and thus the efficiency of the fiber-matrix interface in FRCPC. To support the experimental data, we employed a numerical FE model with specific interfacial constitutive laws to analyze the pull-out process in detail. We suggest two types of the interfacial constitutive laws consisting of either two or three pull-out phases with a quadratic slip-hardening characteristic in the frictional pull-out phase. The former deals with the PVA fibers with a negligible debonding stage relative

to the final slippage, while the latter is concerned with modeling the complete pull-out process of PVA fibers which reveal a significant debonding stage. A FE model is developed with a distinct representation of the fiber, matrix and interface.

The two-phase TSL for the interface between fiber and matrix includes the linear and frictional phases of the pull-out process, whereas the three-phase TSL also describes the debonding stage. We argue that the debonding stage can be ignored specifically for PVA fibers with small diameters and embedded lengths, but in the tests presented in this paper we observed a significant debonding phase. Hence, we suggest a three-phase TSL to numerically model the complete pull-out process. The numerical model is capable of capturing all three main phases of the pull-out process, *i.e.* the elastic, debonding and frictional pull-out phases. Calibration of the model parameters was performed for a single fiber embedded length and its predictive capability was demonstrated for different fiber embedded lengths. The interface models developed in our study are idealizations of a more complicated situation. Nevertheless, they provide the basis to develop sophisticated numerical models to capture the complex relationship between physicochemical properties of incorporated fibers and the efficacy of fiber reinforcement in calcium phosphate cement matrices. These models will enable efficient optimization of the mechanical performance of fiber-reinforced calcium phosphate cements, thereby contributing to the development of novel bioceramic cements with load-bearing capacity.

5. Acknowledgments

The research leading to these results has received funding from the Netherlands Organization for Scientific Research (NWO), VIDI project 13455.

References

[1] J. Zhang, W. Liu, V. Schnitzler, F. Tancret, J.-M. Bouler, Calcium phosphate cements for bone substitution: Chemistry, handling and mechanical properties, Acta Biomaterialia 10 (3) (2014) 1035–1049.

[2] M.-P. Ginebra, M. Espanol, E. B. Montufar, R. A. Perez, G. Mestres, New processing approaches in calcium phosphate cements and their applications in regenerative medicine, Acta Biomaterialia 6 (8) (2010) 2863–2873.

[3] M. Epple, K. Ganesan, R. Heumann, J. Klesing, A. Kovtun, S. Neumann, V. Sokolova, Application of calcium phosphate nanoparticles in biomedicine, Journal of Materials Chemistry 20 (1) (2010) 18–23.

[4] L. L. Hench, J. Wilson, An Introduction To Bioceramics, World Scientific, 1993.

[5] E. Sanzana, M. Navarro, F. Macule, S. Suso, J. Planell, M. Ginebra, Of the in vivo behavior of calcium phosphate cements and glasses as bone substitutes, Acta Biomaterialia 4 (6) (2008) 1924–1933.

[6] R. O'Neill, H. McCarthy, E. Montufar, M.-P. Ginebra, D. I. Wilson, A. Lennon, N. Dunne, Critical review: Injectability of calcium phosphate pastes and cements, Acta Biomaterialia 50 (2017) 1–19.

[7] R. LeGeros, Calcium phosphate materials in restorative dentistry: A review, Advances in Dental Research 2 (1) (1988) 164–180.

[8] J. Osborn, H. Newesely, The material science of calcium phosphate ceramics, Biomaterials 1 (2) (1980) 108–111.

[9] T. Thamaraiselvi, S. Rajeswari, Biological evaluation of bioceramic materials - a review, Carbon 24 (31) (2004) 172.

[10] R. Martin, P. Brown, Mechanical properties of hydroxyapatite formed at physiological temperature, Journal of Materials Science: Materials in Medicine 6 (3) (1995) 138–143.

[11] E. Morgan, D. Yetkinler, B. Constantz, R. Dauskardt, Mechanical properties of carbonated apatite bone mineral substitute: strength, fracture and fatigue behaviour, Journal of Materials Science: Materials in Medicine 8 (9) (1997) 559–570.

[12] R. K. Nalla, J. Kinney, R. O. Ritchie, Mechanistic fracture criteria for the failure of human cortical bone, Nature Materials 2 (3) (2003) 164.

[13] L. A. Dos Santos, L. C. De Oliveira, E. C. da Silva Rigo, R. G. Carrodéguas, A. O. Boschi, A. C. Fonseca de Arruda, Fiber reinforced calcium phosphate cement, Artificial Organs 24 (3) (2000) 212–216.

[14] D.-G. Petre, N. W. Kucko, A. Abbadessa, T. Vermonden, A. Polini, S. C. Leeuwenburgh, Surface functionalization of polylactic acid fibers with alendronate groups does not improve the mechanical properties of fiber-reinforced calcium phosphate cements, Journal of the Mechanical Behavior of Biomedical Materials 90 (2019) 472–483.

[15] Y. Zuo, F. Yang, J. G. Wolke, Y. Li, J. A. Jansen, Incorporation of biodegradable electrospun fibers into calcium phosphate cement for bone regeneration, Acta biomaterialia 6 (4) (2010) 1238–1247.

[16] S. Garcia, A. E. Naaman, J. Pera, Experimental investigation on the potential use of poly (vinyl alcohol) short fibers in fiber-reinforced cement-based composites, Materials and Structures 30 (1) (1997) 43–52.

[17] S. Jiang, S. Liu, W. Feng, PVA hydrogel properties for biomedical application, Journal of the Mechanical Behavior of Biomedical Materials 4 (7) (2011) 1228–1233.

[18] N. W. Kucko, S. de Lacerda Schickert, T. Sobral Marques, R.-P. Herber, J. J. J. P. van den Beuken, Y. Zuo, S. C. G. Leeuwenburgh, Tough and osteocompatible calcium phosphate cements reinforced with poly(vinyl alcohol) fibers (2018) Under Review.

[19] R. Krüger, J. Groll, Fiber reinforced calcium phosphate cements–on the way to degradable load bearing bone substitutes?, Biomaterials 33 (25) (2012) 5887–5900.

[20] S. Wang, V. C. Li, Polyvinyl alcohol fiber reinforced engineered cementitious composites: material design and performances, in: RILEM PRO, Vol. 49, 2006.

[21] A. Bentur, S. Mindess, Fibre Reinforced Cementitious Composites, 2nd Edition, London: CRC Press, 2006.

[22] S. Fu, B. Zhou, X. Chen, C. Xu, G. He, C. Lung, Some further considerations of the theory of fibre debonding and pull-out from an elastic matrix. Part 1: Constant interfacial frictional shear stress, Composites 24 (1) (1993) 5–11.

[23] L. F. Friedrich, C. Wang, Continuous modeling technique of fiber pullout from a cement matrix with different interface mechanical properties using finite element program, Latin American Journal of Solids and Structures 13 (10) (2016) 1937–1953.

[24] Y. Wang, S. Backer, V. C. Li, A special technique for determining the critical length of fibre pull-out from a cement matrix, Journal of Materials Science Letters 7 (8) (1988) 842–844.

[25] A. E. Naaman, G. G. Namur, J. M. Alwan, H. S. Najm, Fiber pullout and bond slip. I: Analytical study, Journal of Structural Engineering 117 (9) (1991) 2769–2790.

[26] A. E. Naaman, G. G. Namur, J. M. Alwan, H. S. Najm, Fiber pullout and bond slip. II: Experimental validation, Journal of Structural Engineering 117 (9) (1991) 2791–2800.

[27] R. J. Kerans, T. A. Parthasarathy, Theoretical analysis of the fiber pullout and pushout tests, Journal of the American Ceramic Society 74 (7) (1991) 1585–1596.

[28] C. Scheffler, S. Zhandarov, W. Jenschke, E. Mäder, Poly (vinyl alcohol) fiber reinforced concrete: investigation of strain rate dependent interphase behavior with single fiber pullout test under quasi-static and high rate loading, Journal of Adhesion Science and Technology 27 (4) (2013) 385–402.

[29] Z. Lin, T. Kanda, V. C. Li, On interface property characterization and performance of fiber reinforced cementitious composites, Concrete Sience and Engineering 1 (1999) 173–184.

[30] R. Breitenbücher, G. Meschke, F. Song, Y. Zhan, Experimental, analytical and numerical analysis of the pullout behaviour of steel fibres considering different fibre types, inclinations and concrete strengths, Structural Concrete 15 (2) (2014) 126–135.

[31] T. Abu-Lebdeh, S. Hamoush, B. Zornig, Rate effect on pullout behavior of steel fibers embedded in very-high strength concrete, American Journal of Engineering and Applied Sciences 3 (2) (2010) 454–463.

[32] E. Vos, H. Reinhardt, Influence of loading rate on bond behaviour of reinforcing steel and prestressing strands, Matériaux et Construction 15 (1) (1982) 3–10.

[33] N. Banthia, J.-F. Trottier, Micromechanics of steel fiber pull-out: Rate sensitivity at very low temperatures, Cement and Concrete Composites 14 (2) (1992) 119–130.

[34] S. Zhandarov, E. Pisanova, K. Schneider, Fiber-stretching test: A new technique for characterizing the fiber–matrix interface using direct observation of crack initiation and propagation, Journal of Adhesion Science and Technology 14 (3) (2000) 381–398.

[35] C. C. Li, G. Kristjansson, A. H. Høien, Critical embedment length and bond strength of fully encapsulated rebar rockbolts, Tunnelling and Underground Space Technology 59 (2016) 16–23.

[36] M. Alberti, A. Enfedaque, J. Gálvez, A. Ferreras, Pull-out behaviour and interface critical parameters of polyolefin fibres embedded in mortar and self-compacting concrete matrixes, Construction and Building Materials 112 (2016) 607–622.

[37] J. K. Morrison, S. P. Shah, Y.-S. Jenq, Analysis of fiber debonding and pullout in composites, Journal of Engineering Mechanics 114 (2) (1988) 277–294.

[38] T. Abu-Lebdeh, S. Hamoush, W. Heard, B. Zornig, Effect of matrix strength on pullout behavior of steel fiber reinforced very-high strength concrete composites, Construction and Building Materials 25 (1) (2011) 39–46.

[39] Z. Lin, V. C. Li, Crack bridging in fiber reinforced cementitious composites with slip-hardening interfaces, Journal of the Mechanics and Physics of Solids 45 (5) (1997) 763–787.

[40] Y. Wang, V. C. Li, S. Backer, Modelling of fibre pull-out from a cement matrix, International Journal of Cement Composites and Lightweight Concrete 10 (3) (1988) 143–149.

[41] J. Alwan, A. E. Naaman, W. Hansen, Pull-out work of steel fibers from cementitious composites: Analytical investigation, Cement and Concrete Composites 13 (4) (1991) 247–255.

[42] S. Zhandarov, E. Mäder, An alternative method of determining the local interfacial shear strength from force–displacement curves in the pull-out and microbond tests, International Journal of Adhesion and Adhesives 55 (2014) 37–42.

[43] S. Zhandarov, E. Mäder, Peak force as function of the embedded length in pull-out and microbond tests: Effect of specimen geometry, Journal of Adhesion Science and Technology 19 (10) (2005) 817–855.